

RESEARCH

Open Access



Evaluation of functional magnetic resonance APT and DKI imaging for breast cancer

Haiyan Shan^{2†}, Tengfei Ke^{1†}, Shasha Bao^{2†}, Yifan Liu¹, Na Tan², Xinyan Zhou², Guochen Li², Guangrong Zheng², Yongzhou Xu³, Yu Xie¹, Chengde Liao^{2*} and Jun Yang^{1*}

Abstract

Objective This study aimed to compare the performance of amide proton transfer-weighted imaging (APTWI) and diffusion kurtosis imaging (DKI) in differentiating benign from malignant breast lesions, evaluate molecular subtypes of breast cancer, and determine the diagnostic efficacy of the quantitative magnetic resonance imaging (qMRI) parameters in differentiating benign from malignant breast diseases.

Methods The study included 168 women who underwent breast APTWI and DKI at Yunnan Cancer Hospital between December 2022 and July 2023. The APT signal intensity (SI), apparent kurtosis coefficient (Kapp), non-Gaussian diffusion coefficient (Dapp), and apparent diffusion coefficient (ADC) values were measured before surgery. The differences in the aforementioned qMRI parameters in molecular subtypes of breast cancer were analyzed using one-way analysis of variance. The efficacy of each quantitative parameter in differentiating benign from malignant breast diseases was evaluated using the receiver-operating characteristic curve.

Results Significant differences in qMRI parameters were noted between benign and malignant breast lesions. The Kapp ($P < .0001$) and APT ($P < .05$) values were higher for malignant tumors than for benign lesions. Conversely, the ADC ($P < .0001$) and Dapp ($P < .0001$) values were lower for malignant tumors than for benign lesions. The diagnostic performance was assessed using the area under the curve (AUC) for various parameter combinations. The AUC of Kapp was 0.871, Dapp was 0.872, APT SI was 0.643, DKI + APT was 0.893, DKI + ADC was 0.936, APT + ADC was 0.925, and DKI + APT + ADC was 0.933. Additionally, ADC values ($P = .01$) demonstrated superior diagnostic performance compared to Kapp ($P = .03$), Dapp ($P = .03$), and APT values ($P = .06$) in distinguishing between different molecular subtypes of breast cancer.

Conclusions APTWI distinguished benign from malignant breast disease and enhanced the utility of diffusion-weighted MRI. However, it was not superior to DKI and DWI in identifying the molecular subtypes of breast cancer.

Keywords Amide proton transfer-weighted imaging, Breast cancer, Diffuse kurtosis imaging, Diffusion-weighted imaging, Quantitative molecular resonance imaging

[†]Haiyan Shan, Tengfei Ke and Shasha Bao are co-first authors.

*Correspondence:

Chengde Liao
chengdeliao@qq.com
Jun Yang
jmdyang@qq.com

¹Department of Radiology, The Third Affiliated Hospital of Kunming Medical University, Yunnan Cancer Hospital/Center, No. 519 Kunzhou Road, Xishan District, Kunming, Yunnan 650118, P.R. China

²Department of Radiology, Yan 'an Hospital Affiliated to Kunming Medical University, Yan 'an Hospital of Kunming City, Kunming, China

³Philips Healthcare, Kunming, China



Introduction

Breast cancer is the most prevalent form of cancer among women, affecting 1 in 20 women globally. Its incidence continues to increase [1]. In 2020, female breast cancer has surpassed lung cancer as the most commonly diagnosed cancer, with an estimated 2.3 million new cases [2]. Despite progress in diagnosing and treating breast cancers, the prognosis for biologically aggressive or advanced cases remains poor. Breast malignancy is a complex and diverse disease, with distinct subtypes displaying various biologic characteristics and responses to various treatments, leading to diverse clinical outcomes [3, 4]. Appropriate predictive and prognostic tools are needed for decision-making and treatment selection to optimize the management of breast cancer.

Magnetic resonance imaging (MRI) is widely used for diagnosing and assessing prognosis in breast cancer due to its excellent soft tissue resolution and noninvasive nature. Advanced quantitative MRI (qMRI) techniques have enhanced diagnostic capabilities for breast diseases. Diffusion kurtosis imaging (DKI) is a specialized diffusion-weighted imaging (DWI) technique proposed by Jensen et al. in 2005 [5]. DWI is a medical imaging technique that uses the random movement (diffusion) of water molecules in tissues to produce images. The apparent diffusion coefficient (ADC) value is calculated from the DWI images and used to quantify the degree of free diffusion of water molecules in tissues [6]. Compared to traditional DWI, DKI offers higher sensitivity and multiple b-values, which can facilitate the analysis of certain characteristics of tumor tissue and promote the classification of tumor tissue types [7, 8]. DKI is involved in advanced pathology research and facilitates disease classification [9]. In clinical studies, DKI focused on neurologic diseases [10], although it has also been used to diagnose and evaluate solid malignancies, such as liver cancer [11], prostate cancer [12], and endometrial cancer [13]. The technique has high diagnostic efficacy and can help evaluate the degree of diffusion and microstructure characteristics of tumor tissues, thus providing a reference for the quantitative diagnosis and formulation of treatment strategies.

Amide proton transfer-weighted imaging (APTWI) is an imaging method proposed by Zhou et al. [14] in 2013 to evaluate the chemical transfer properties of amide protons at the 3.5-ppm chemical shift [15]. APTWI is highly sensitive to subtle pathologic tissue changes and can detect changes that cannot be determined using conventional MRI methods. It can provide information on the molecular composition of tissues, protein content, and the dynamic process of amide protons in tissues, which is valuable in evaluating the microstructure and chemical environment of tissues [16, 17]. Compared with other MRI techniques, APTWI requires no injection of

contrast agents and is less invasive to the patient. Hence, it is safer and more acceptable. APTWI is widely used in evaluating stroke, white matter diseases, tumors, neurodegenerative diseases, and other disorders. However, few studies have reported on the use of APTWI in distinguishing between benign and malignant breast lesions and evaluating the molecular subtypes of breast cancer. The reliability of the amide proton transfer signal intensity (APT SI) parameter and DKI-derived parameters in assessing breast diseases has not been explored yet.

Therefore, this study aimed to compare the role of DKI, DWI, and APTWI in differentiating benign from malignant breast lesions, evaluating molecular subtypes of breast cancer, and determining the diagnostic significance of the obtained parameters in various prognostic factors of the disease. It is hoped that this new information will provide new ideas for the diagnosis, treatment, and outcome of breast cancer.

Materials and methods

Patients

This retrospective study was approved by The Third Affiliated Hospital of Kunming Medical University (Yunnan Cancer Hospital), and informed consent was obtained from all study participants.

This study included 202 patients who underwent DKI and APTWI in Yunnan Cancer Hospital from December 2022 to July 2023. Furthermore, 34 patients were excluded because of the following reasons: received preoperative chemotherapy ($n=1$), poor image quality ($n=14$), unknown pathologic results of puncture ($n=15$), or no surgery ($n=4$). Finally, 168 patients with breast diseases were included in this study, of which 55 patients had benign lesions and 113 had malignant lesions. The molecular subtypes were judged according to the following standards: the 2021 Chinese Society of Clinical Oncology Breast Cancer Guidelines [18]. The patients with breast cancer were classified into 5 groups: luminal A ($n=19$), luminal B1 ($n=55$), luminal B2 ($n=9$), HER-2 overexpression ($n=14$), and triple negative ($n=16$). The expression of HER-2 was negative in luminal B1 and positive in luminal B2. The demographic and clinical data of the included patients are listed in Table 1.

Data acquisition

MRI was performed using a 3.0-T scanner (Ingenia Elition, Philips Healthcare) with a dedicated 8-channel bilateral breast coil. All premenopausal patients were examined during the 2nd week of the menstrual cycle. The patients were placed prone, with feet first and breasts naturally hanging in the center slot of the coil. Routine sequence scans, including T1-weighted imaging (T1WI), T2-weighted imaging (T2WI), and DWI, were performed first. Subsequently, the DKI and APTWI sequences were

Table 1 Baseline demographic and clinical characteristics of included patients with breast disease

Characteristic	Benign lesions (n=55)	Malignant lesions (n=113)	P value
Patient characteristic			
Patient age (year)	45.2 ± 8.7	48.7 ± 9.0	0.017
Menstrual status			
Premenopausal (n=104)	40 (72.7%)	64 (56.6%)	0.044
Postmenopausal (n=64)	15 (27.3%)	49 (43.3%)	
Lesion characteristic			
0.0486			
Size (cm)	2.72 ± 2.21	3.35 ± 1.72	
Masses	28 (50.9%)	96 (85.0%)	
Shape			
<0.0001			
Oval or round (n=45)	37 (67.3%)	8 (7.1%)	
Irregular (n=123)	18 (32.7%)	105 (92.9%)	
Kinetic curve type			
<0.0001			
Persistent	9	0	
Plateau	22	12	
Washout	12	98	
Others	12	3	
BI-RADS			
<0.0001			
Negative (categories 1, 2, and 3)	31 (56.4%)	0 (0.0%)	
Positive (categories 4, 5, and 6)	18 (32.7%)	113 (100.0%)	
Parameters			
Kapp	0.53 ± 0.20	0.92 ± 0.31	<0.0001
Dapp (×10 ⁻³ mm ² /s)	1.98 ± 0.65	1.15 ± 0.52	<0.0001
MTRasym (3.5 ppm)	2.27 ± 1.36	2.78 ± 1.24	0.0173
ADC (×10 ⁻³ mm ² /s)	1.46 ± 0.46	0.79 ± 0.24	<0.0001

ADC, apparent diffusion coefficient; BI-RADS, breast imaging reporting and data system; Dapp, apparent diffusivity; Kapp, apparent kurtosis coefficient; MTRasym (3.5 ppm), asymmetric magnetization transfer ratio at 3.5 ppm

obtained with reference to the routine sequence images under the guidance of an experienced radiologist, to detect all sections containing tumor tissue. The DKI and APT examinations were performed before administering the contrast agent to avoid the agent interfering with the APTWI signal. The scanning scheme is presented in Table 2.

Table 2 MRI scanning parameters

Parameters	T1WI	T2WI	DWI	DKI	APTWI	DCE-MRI
Sequence	TSE	TSE	EPI	EPI	TSE	
Orientation	Axial	Axial	Axial	Axial	Axial	Axial
TR/TE(ms)	471/13	4,000/70	10,000/74	10,000/89	3,975/8.8	4.8/2.1
FOV	280 × 340	280 × 340	340 × 340	340 × 340	230 × 279	280 × 345
Matrix	280 × 337	280 × 319	128 × 128	136 × 144	128 × 155	320 × 320
Slice thickness	4	4	4	4	6	1
Slice number	36	36	36	36	6	360
NSA	2	2	1	1	1	1
Fat suppression	SPAIR	SPAIR	SPAIR	SPAIR	SPAIR	SPAIR
b value (s/mm ²)	/	/	/	0, 1000, 1500, 2000	/	/
Scan time	2 min 10 s	2 min 48 s	2 min 20 s	8 min	4 min 14 s	9 min 10 s

Note APTWI, amide proton transfer-weighted imaging; DCE, dynamic enhanced magnetic resonance; DKI, diffusion kurtosis imaging; DWI, diffusion-weighted imaging; EPI, echo planar imaging; FOV, field of view; NSA, number of signal average; TR/TE, repetition time/echo time; TSE, turbo spin echo; SPAIR, spectral adiabatic inversion recovery; T1WI, T1-weighted imaging; T2WI, T2-weighted imaging

Data analysis

The obtained APTWI images were postprocessed with the Philips IntelliSpace Portal workstation. First, the solid part of the tumor tissue was sketched on the axial DWI image, and the region of interest (ROI) was sketched with the plain scan and enhanced sequences as references. Next, the false-color images of APTWI parameters were merged with the DWI images. The range of ROI mapping depended on the size of the tumor, ensuring avoidance of the location of bleeding, necrosis, and cystic degeneration. The specific APT SI value was defined as the APT signal measured at 3.5 ppm. The calculation formula for APT imaging was $MTR_{asym}(3.5\text{ ppm}) = [S_{sat}(-3.5\text{ ppm}) - S_{sat}(+3.5\text{ ppm})] / S_0$, where $MTR_{asym}(3.5\text{ ppm})$ is the asymmetric magnetization transfer ratio at 3.5 ppm, S_{sat} is the signal strength after the saturated pulse is applied, and S_0 is the signal strength without the application of the saturated pulse. The maximum diameter and morphological characteristics of lesions were recorded according to the consensus-based breast imaging reporting and data system [19]. The obtained DKI data were processed with Medical Imaging Interaction Toolkit (MITK) diffusion software. The formula used for calculating the DKI parameters was $S_b = S_0 \times \exp(-b \times D_{app} + b^2 \times D_{app}^2 \times Kapp / 6)$, where S_b represents the SI under various b values and D_{app} is the mean diffusivity. D_{app} represents the non-Gaussian diffusion coefficient, and the apparent kurtosis coefficient (Kapp) represents the degree of deviation from the Gaussian distribution. These measurements were conducted by 2 Radiologists with 5 and 10 years of experience, respectively, in diagnosing breast lesions, both of whom were unaware of the histopathologic findings. The final values of the measurements of each lesion were the average values of the corresponding measurements of each section.

Histopathologic analysis

Two pathologists with 5 and 12 years of experience, respectively, independently analyzed the hematoxylin–eosin-stained and immunohistochemical tissue specimens. The histopathologic results were based on consensus, with differences resolved by discussion. The criteria for interpreting ER and PR statuses were as follows: $\geq 10\%$ of tumor cells with positive staining were ER and PR positive, and $< 10\%$ of negative tumor cells were positive staining [20]. The test criteria for HER-2 were as follows: samples with + and – signals were negative, and samples with +++ signals were positive. The samples with ++ signal were hybridized in situ (Fish in situ hybridization experiment). A sample with gene amplification was defined as positive, and a sample without gene amplification was defined as negative [21]. The expression criteria of Ki-67 were as follows: $\geq 14\%$, high-expression tumor cells staining positive, and $< 14\%$ tumor cells staining positive, negative expression [22]. The status of lymph nodes was determined according to the pathologic results of lymph node specimens.

Statistical analysis

Data analysis was performed with software (SPSS software version 26.0, IBM; GraphPad Prism version 9.0). Inter-observer reliability, consistency of measurements, normality of data, and differences between benign and malignant groups were assessed using the intraclass correlation coefficient, Bland–Altman plots, Kolmogorov–Smirnov test, and t-tests, χ^2 tests, or Fisher's exact tests, respectively. Variations in qMRI parameters across breast cancer subtypes were analyzed with ANOVA and least significant difference method, while ROC curves and Delong's test evaluated diagnostic parameters. Logistic regression analyzed multiple indicators, considering $P < .05$ as statistically significant.

Results

Participant characteristics

The study initially enrolled 202 participants. During the selection process, 34 participants were excluded for various reasons: 1 patient underwent preoperative chemotherapy, 14 had poor image quality, 15 had missing pathologic results, and 4 had not undergone surgery. Thus, 168 patients with breast diseases were included in the study and classified according to their histopathologic results. Lesions in 55 patients were diagnosed as benign, and those in 113 as malignant. Figure 1 illustrates the flow chart of the participant selection process.

Consistency test

The agreement between the 2 observers was satisfactory. The intraclass correlation coefficients for APT SI, Kapp, Dapp, and ADC are 0.997, 0.947, 0.787, and 0.989, respectively. For each of these qMRI parameters, the Bland–Altman test confirmed a high level of agreement between the 2 observers. Only a few values for each parameter exceeded the 95% agreement limit, as illustrated in Fig. 2. Therefore, the average values of the parameters measured by the 2 observers were considered the final evaluation indices.

Comparison of quantitative parameters of magnetic resonance

The ADC and Dapp values were higher, whereas the Kapp and APT SI values were lower, in patients with benign lesions than in those with malignancies (Table 1; Fig. 3). Furthermore, the Kapp value was higher and the Dapp and ADC values were lower in the ER-positive group than in the ER-negative group. The Kapp value was higher in the PR-positive group than in the PR-negative group, and Dapp and ADC values were lower in the PR-positive group than in the PR-negative group. The APT SI

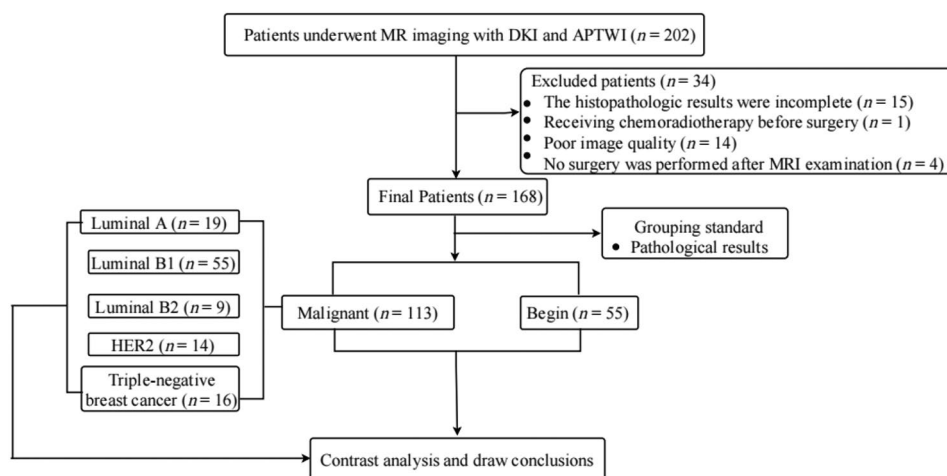


Fig. 1 Flow diagram of the patient selection process. APTWI, Amide proton transfer–weighted imaging; DKI, diffusion kurtosis imaging; HER-2, human epidermal growth factor receptor-2

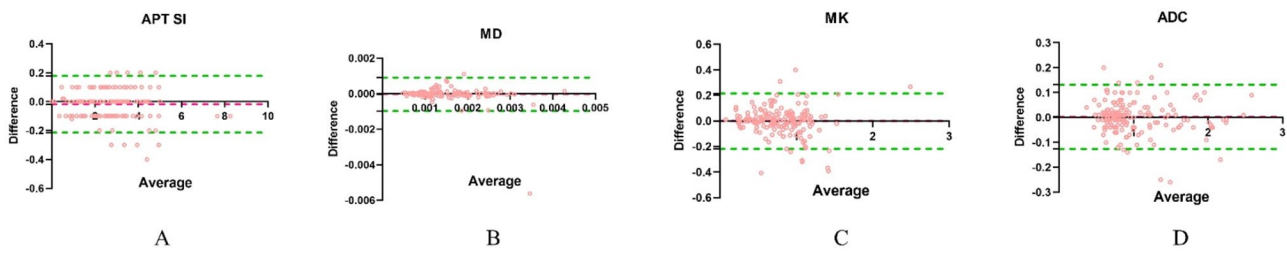


Fig. 2 Bland–Altman plots presenting the distribution of the differences in APT SI (A), MD (B), MK (C), and ADC (D) between the 2 observers. The red horizontal solid line represents the mean difference, and the 2 green horizontal lines represent the limits of agreement. ADC, apparent diffusion coefficient; APT SI, amide proton transfer signal intensity; MD, mean diffusivity; MK, mean kurtosis

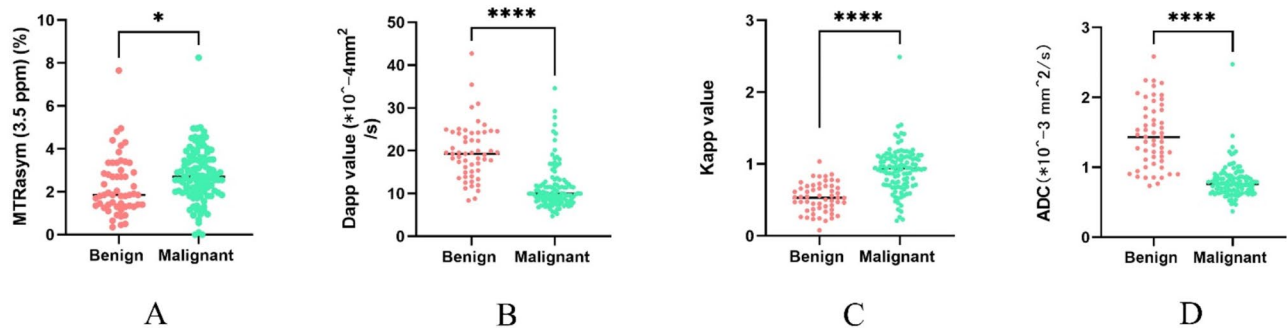


Fig. 3 MTRasym (3.5 ppm), Dapp, Kapp, and ADC values in benign and malignant lesions. (A) MTRasym (3.5 ppm) value (%) was lower in the benign group (2.27 ± 1.36) than in the malignant group (2.78 ± 1.24). (B) Dapp value ($\times 10^{-3} \text{ mm}^2/\text{s}$) was higher in the benign group (1.98 ± 0.65) than in the malignant group (1.15 ± 0.52). (C) Kapp value was lower in the benign group (0.53 ± 0.20) than in the malignant group (0.92 ± 0.31). (D) ADC value ($\times 10^{-3} \text{ mm}^2/\text{s}$) was higher in the benign group (1.46 ± 0.46) than in the malignant group (0.79 ± 0.24). ** means $P < .01$, **** means $P < .0001$. ADC, apparent diffusion coefficient; Dapp, mean diffusivity; Kapp, apparent kurtosis coefficient; MTRasym (3.5 ppm), asymmetric magnetization transfer ratio at 3.5 ppm

Table 3 Comparison of parameters among prognostic factors of breast cancer

Factors	Number of patients	Kapp	P value	Dapp	P value	MTRasym	P value	ADC	P value
ER			0.005		0.0038		0.8770		0.0015
positive	80	0.97 ± 0.33		1.06 ± 0.47		2.77 ± 1.27		0.75 ± 0.16	
negative	33	0.80 ± 0.21		1.36 ± 0.57		2.81 ± 1.18		0.90 ± 0.34	
PR			0.0137		0.0361		0.9912		0.0060
positive	76	0.97 ± 0.33		1.08 ± 0.49		2.78 ± 1.27		0.75 ± 0.18	
negative	37	0.82 ± 0.23		1.29 ± 0.56		2.78 ± 1.18		0.88 ± 0.32	
HER-2			0.0801		0.2400		0.0251		0.0545
positive	23	0.82 ± 0.18		1.26 ± 0.38		2.27 ± 1.10		0.88 ± 0.22	
negative	90	0.95 ± 0.33		1.12 ± 0.55		2.91 ± 1.24		0.77 ± 0.24	
Ki-67			0.5422		0.4192		0.3236		0.1672
positive	92	0.93 ± 0.25		1.13 ± 0.51		2.72 ± 1.15		0.78 ± 0.24	
negative	21	0.87 ± 0.49		1.23 ± 0.55		3.02 ± 1.57		0.86 ± 0.23	
Lymph node status			0.0470		0.6695		0.6269		0.1593
positive	74	0.97 ± 0.32		1.13 ± 0.54		2.80 ± 1.28		0.77 ± 0.25	
negative	37	0.84 ± 0.28		1.12 ± 0.50		2.68 ± 1.12		0.84 ± 0.22	
Tumor diameter			0.0537		0.6389		0.6530		0.5961
$\geq 2 \text{ cm}$	96	0.95 ± 0.30		1.16 ± 0.52		2.80 ± 1.20		0.80 ± 0.25	
$< 2 \text{ cm}$	17	0.79 ± 0.31		1.09 ± 0.51		2.65 ± 1.50		0.76 ± 0.18	

Note ADC, apparent diffusion coefficient; Dapp, apparent diffusivity; ER, estrogen receptor; HER-2, human epidermal growth factor receptor-2; Kapp, apparent kurtosis coefficient; MTRasym (3.5 ppm), asymmetric magnetization transfer ratio at 3.5 ppm; PR, progesterone receptor

value was lower in the HER-2-positive group than in the HER-2-negative group, and the Kapp value was higher in the HER-2-positive group with lymph node metastasis than in the HER-2-negative group (Table 3).

Regarding the molecular subtypes of breast cancer, statistically significant differences in the Dapp, Kapp, and ADC values were noted among the 5 groups, but no statistically significant differences were noted in the APT

Table 4 Comparisons of the parameters derived from APT imaging and DKI among breast cancer subtypes

Parameters	Luminal A (n=19)	Luminal B1 (n=55)	Luminal B2 (n=9)	HER-2+ (n=14)	TNBC (n=16)	P value
MD ($\times 10^{-3}$ mm ² /s)	1.20 ± 0.56	1.02 ± 0.46	1.00 ± 0.28	1.42 ± 0.35	1.34 ± 0.73	0.0302
MK	0.91 ± 0.51	1.00 ± 0.26	0.96 ± 0.14	0.74 ± 0.14	0.83 ± 0.25	0.0325
MTRasym ($\times 10^{-3}$ mm ² /s)	3.16 ± 1.58	2.71 ± 1.17	2.05 ± 0.69	2.40 ± 1.30	3.31 ± 0.90	0.0645
ADC ($\times 10^{-3}$ mm ² /s)	0.83 ± 0.22	0.79 ± 0.26	0.79 ± 0.26	0.93 ± 0.17	0.88 ± 0.45	0.0106

Note ADC, apparent diffusion coefficient; HER-2, human epidermal growth factor receptor-2; MD, mean diffusivity; MK, mean kurtosis; MTRasym, asymmetric magnetization transfer ratio; TNBC, triple-negative breast cancer

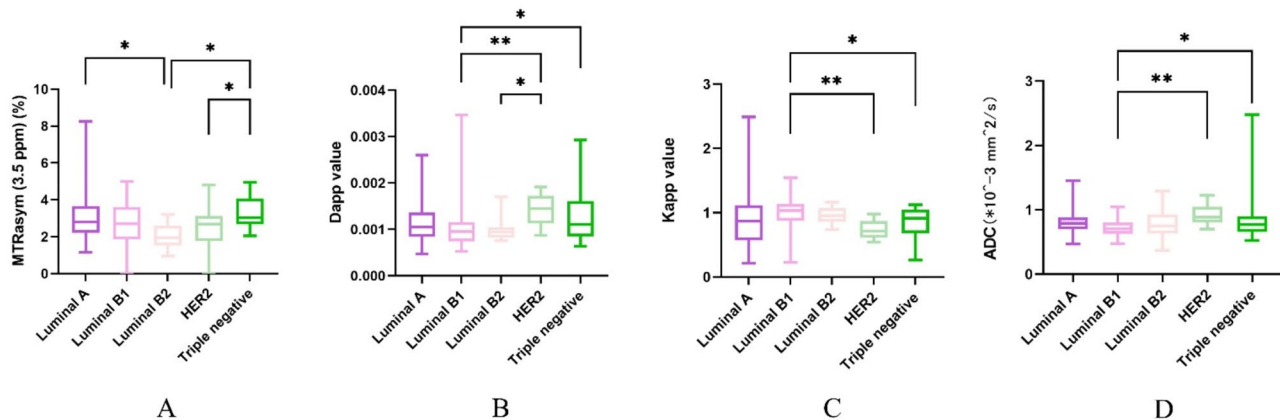


Fig. 4 Boxplots illustrate MTRasym (3.5 ppm)(A), Dapp(B), Kapp(C), and ADC(D) in molecular subtypes of breast cancer. * $P < .05$, ** $P < .01$. ADC, apparent diffusion coefficient; Dapp, apparent diffusivity; Kapp, apparent kurtosis coefficient; MTRasym (3.5 ppm), asymmetric magnetization transfer ratio at 3.5 ppm

SI value, as indicated in Table 4; Fig. 4. These findings suggested that the APT SI values failed to demonstrate superior diagnostic performance compared with DKI and ADC in distinguishing between the various molecular subtypes of breast cancer. Figures 5 and 6 illustrate cases of typical MRI scans and pathologic findings of a patient with malignant invasive breast cancer and a patient with benign fibroadenoma, respectively.

Comparison of the ROC curves

The ROC curve analysis of benign and malignant breast lesions is illustrated in Fig. 7; Table 5. The AUC values of APT SI, Kapp, Dapp, and ADC in distinguishing benign from malignant breast diseases were as follows: AUC (ADC)=0.928, AUC (Dapp)=0.872, AUC (Kapp)=0.871, AUC (APT SI)=0.643, AUC (DKI+ADC)=0.936, AUC (DKI+ADC+APT)=0.933, AUC (APT+ADC)=0.925, and AUC (DKI+APT)=0.893. The ROC curve analysis indicated that certain MRI parameters and their combinations were highly effective in distinguishing between benign and malignant breast lesions. Specifically, the combination of DKI and ADC parameters showed the highest diagnostic accuracy, outperforming other individual or combined parameters. Additionally, these MRI parameters also demonstrated significant effectiveness in evaluating prognostic factors of breast cancer, including

the assessment of lymph node metastasis status (Fig. 8; Table 6).

Discussion

APTWI and DKI imaging have been widely used in diagnosing tumors in various parts of the body. However, to our knowledge, no studies have used DKI, APTWI, and DWI to distinguish benign from malignant breast diseases and evaluate the molecular subtypes of breast cancer. In this study, we observed that the APT SI values in malignant tumors were higher than those in benign lesions, indicating that malignant tumors exhibited rapid cell proliferation, increased protein expression, and high cell density, leading to a higher concentration of mobile proteins and peptides within the tumor compared with benign tumors [23]. Moreover, the Kapp values in the malignant group were higher, and the Dapp and ADC values were lower than those in the benign group. This observation aligns with the findings reported by Meng et al. [24]. The results might be attributed to alterations in the cell structure and heightened tissue heterogeneity in breast malignancies. Benign tumors usually exhibit low diffusion of water, attributed to their orderly cell arrangement, relatively normal tissue structure, and large spaces between cells, which allow for freer diffusion of water molecules [25]. Therefore, benign tumors usually have higher Dapp and ADC values than malignant tumors,

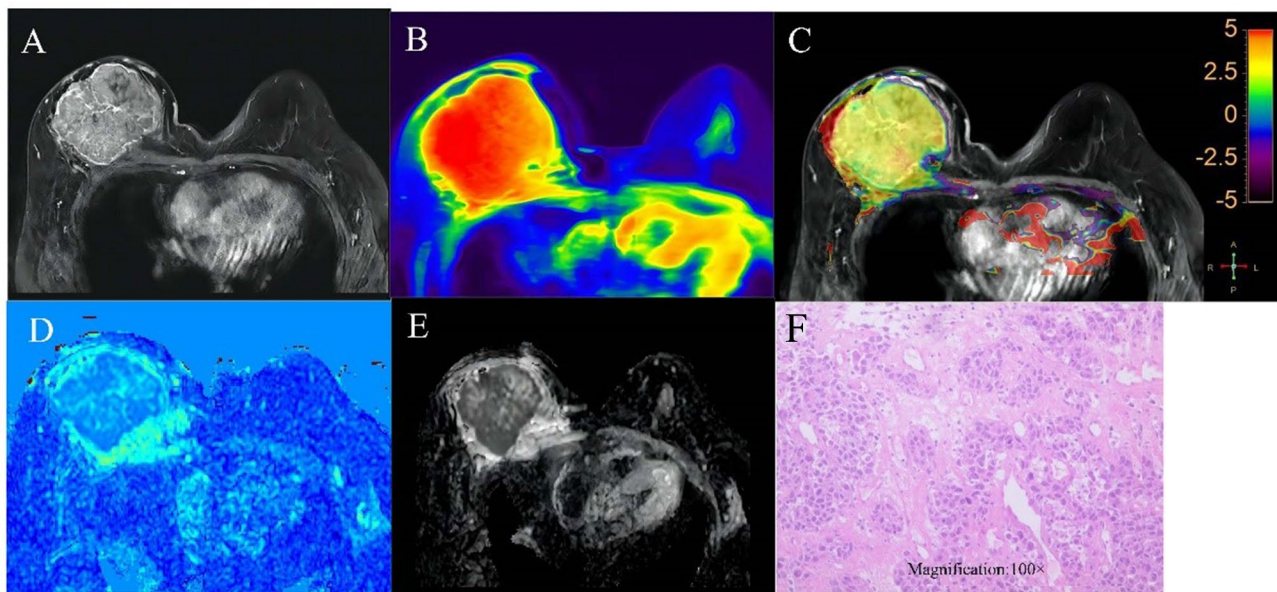


Fig. 5 A 45-year-old woman with high-grade invasive carcinoma in the right breast. **(A)** Dynamic enhanced MR image. **(B)** APT Anatomical Calibration Diagram. The area shown in red on the false color image of the right breast is the tumor area. **(C)** APT Functional and Dynamic Enhancement Fusion imaging. The area shown in yellow on the false color image of the right breast represents the tumor area. **(D)** False-color image of Kapp obtained using DKI processing. **(E)** ADC image. **(F)** Pathologic HE staining result. ADC, apparent diffusion coefficient; APT, amide proton transfer; HE, hematoxylin and eosin

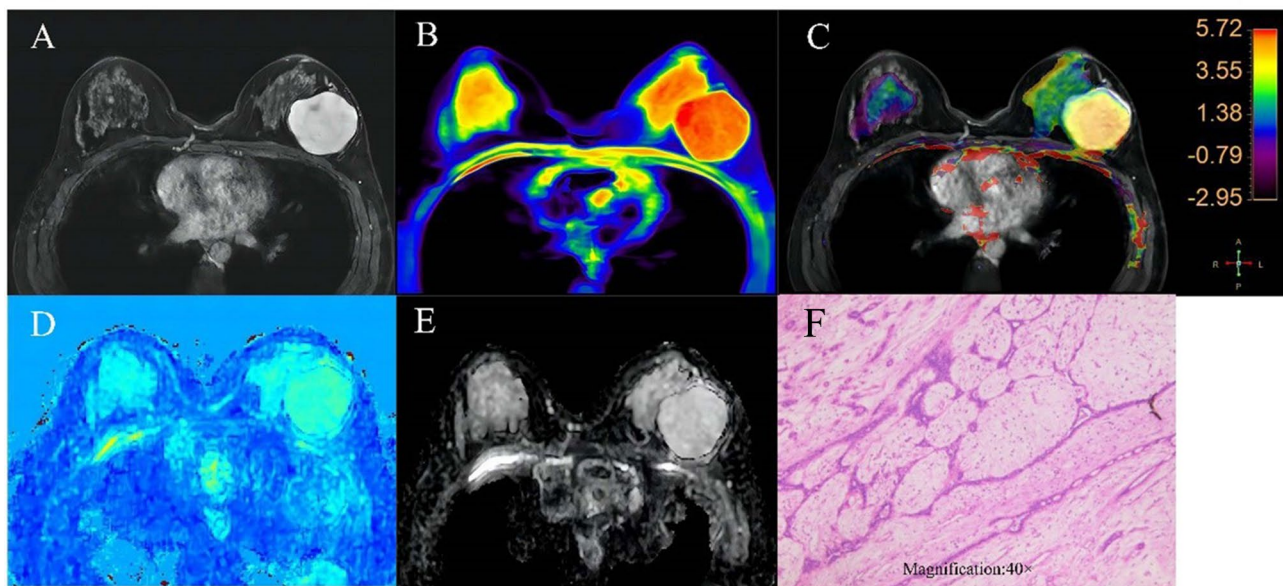


Fig. 6 A 31-year-old woman with a fibroadenoma in the left breast. **(A)** Dynamic enhanced MR image. **(B)** APT Anatomical Calibration Diagram. The area shown in red on the false color image of the left breast is the tumor area. **(C)** APT Functional and Dynamic Enhancement Fusion imaging. The area shown in yellow on the false color image of the left breast represents the tumor area. **(D)** False-color image of Kapp obtained after DKI processing. **(E)** ADC image. **(F)** Pathologic HE staining result. ADC, apparent diffusion coefficient; APT, amide proton transfer; HE, hematoxylin and eosin

and water diffusion is close to a Gaussian distribution [6]. In contrast, the tissue structure loses its normal hierarchy because of the disordered cell arrangement in malignant tumors, and the space between cells is smaller than that in normal tissues. This aberration restricts the free diffusion of water molecules, resulting in deviation from

the Gaussian distribution and, consequently, high Kapp and low ADC values [26].

Accurate preoperative evaluation of the molecular subtypes of breast cancer is essential because various subtypes have diverse clinical treatments and prognosis. This study evaluated the diagnostic potential of APTWI, DKI

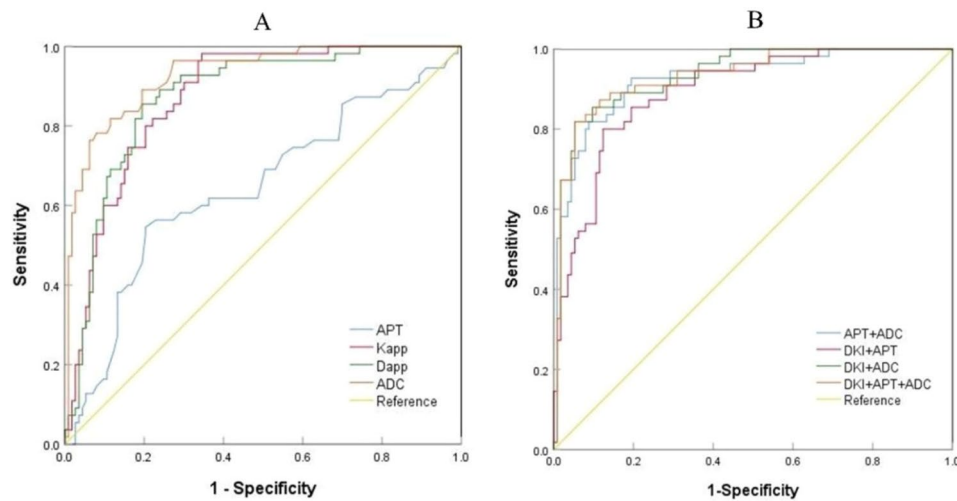


Fig. 7 ROC curves to assess the utility of metrics for distinguishing malignant from benign lesions. **(A)** AUC (Kapp)=0.871, AUC (Dapp)=0.872, AUC (APT)=0.643, AUC (ADC)=0.928. **(B)** AUC (APT + ADC)=0.925, AUC (DKI + APT)=0.893, AUC (DKI + ADC)=0.936, AUC (DKI + ADC + APT)=0.933. ADC, apparent diffusion coefficient; APT, amide proton transfer; AUC, area under the curve; Dapp, apparent diffusivity; DKI, diffusion kurtosis imaging; Kapp, apparent kurtosis coefficient

Table 5 ROC analysis of the diagnostic performance of parameters and methods alone or in combination in distinguishing between benign and malignant breast lesions

Multi parameters	AUC (95%)	P value	Youden index	Sensitivity (%)	Specificity (%)
Parameters					
Kapp	0.871 (0.818–0.924)	<0.0001	0.637	98.2	65.5
Dapp	0.872 (0.816–0.928)	<0.0001	0.660	85.5	80.5
MTRasym	0.643 (0.550–0.735)	0.0027	0.342	54.5	79.6
ADC	0.928 (0.888–0.968)	<0.0001	0.703	81.8	88.5
Combined diagnosis					
DKI + APT	0.893 (0.843–0.942)	<0.0001	0.676	80.0	87.6
DKI + ADC	0.936 (0.898–0.973)	<0.0001	0.765	81.8	94.7
APT + ADC	0.925 (0.881–0.969)	<0.0001	0.733	92.7	80.5
DKI + APT + ADC	0.933 (0.893–0.974)	<0.0001	0.765	81.8	94.7

AUC: Kapp>MTRasym (Z=-4.191, P <.0001), Dapp>MTRasym (3.5 ppm) (Z=-3.943, P <.0001), ADC > MTRasym (Z=-5.677, P <.0001), ADC>Kapp (Z=-2.182, P=.029), ADC>Dapp (Z=-2.358, P=.018); DKI+ADC>DKI+APT (Z=-2.835, P=.005), DKI+APT>DKI+APT+ADC (Z=-2.947, P=.003). No considerable difference in AUCs of other parameters and methods was noted. ADC, apparent diffusion coefficient; APT, amide proton transfer; AUC, area under the curve; Dapp, apparent diffusivity; DKI, diffusion kurtosis imaging; Kapp, apparent kurtosis coefficient; MTRasym (3.5 ppm), asymmetric magnetization transfer ratio at 3.5 ppm

and ADC in identifying the molecular subtypes of breast cancer. The results revealed that DKI and ADC were superior to APTWI in diagnosing the molecular subtypes of breast cancer, and in the differentiation and prognosis of benign versus malignant breast lesions. These distinctions might be attributed to the following factors: (i) The ROI sketched by APT images was obtained from a portion of the tumor, that is, the largest area of the tumor in the image, and only the average was calculated. Therefore, the APTSI value might not have reflected the overall heterogeneity of the tumor, and the main differences between various lesions might have been lost. (ii) The APTWI image postprocessing depended on improved image quality, and no APT imaging sequence existed with standard parameters. (iii) Patients with breast diseases often have breast nodules in an early stage; therefore, the breast lesions in the enrolled patients were small and the secretion of protein polypeptides and other substances might be low. (iii) The difference in water diffusion ratio among populations might be more vital than the difference in protein and peptide contents. For these reasons, the differences between DKI combined with ADC values and APT SI values were pronounced in this study. Moreover, APT SI primarily reflects the exchange process between amide groups and water molecules, which varies across various tissues or lesions. This variability poses relative challenges to differentially diagnosing diseases or lesions using APT.

In clinical practice, the immunohistochemical classification of breast cancers based on ER, PR, HER2, and Ki-67 expression levels is crucial in determining the molecular classification of cancers. The classification provides essential guidance for estimating prognosis

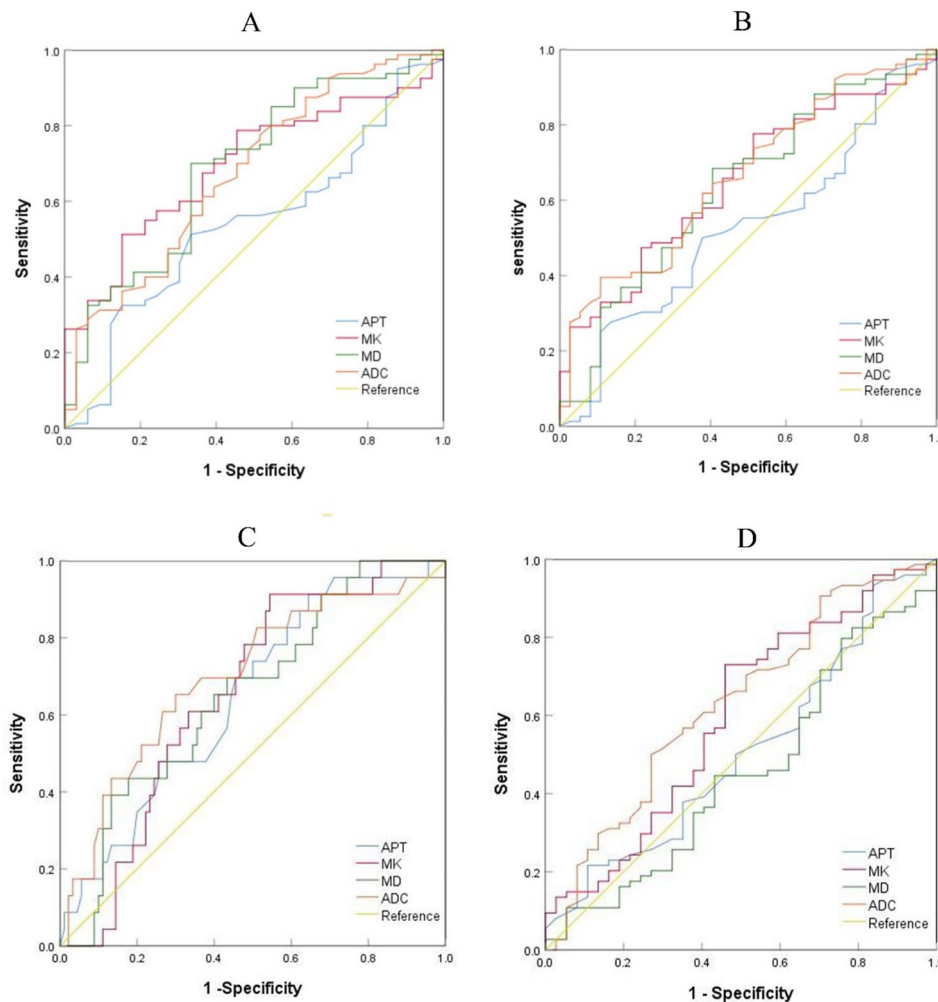


Fig. 8 ROC curves of each quantitative parameter on ER (A), PR (B), HER2 (C), and lymph node metastasis status (D). (A) AUC (Kapp)=0.695, AUC (Dapp)=0.690, AUC (APT)=0.541, and AUC (ADC)=0.677. (B) AUC (Kapp)=0.651, AUC (Dapp)=0.638, AUC (APT)=0.524, and AUC (ADC)=0.665. (C) AUC (Kapp)=0.650, AUC (Dapp)=0.650, AUC (APT)=0.645, and AUC (ADC)=0.699. (D) AUC (Kapp)=0.596, AUC (Dapp)=0.546, AUC (APT)=0.508, and AUC (ADC)=0.629. No considerable difference in AUCs of other parameters and methods was noted. ADC, apparent diffusion coefficient; APT, amide proton transfer; AUC, area under the curve; Dapp, apparent diffusivity; DKI, diffusion kurtosis imaging; Kapp, apparent kurtosis coefficient

and determining treatment [22]. Therefore, we evaluated the diagnostic and prognostic efficacy of several quantitative markers (ER, PR, HER2, Ki-67, and lymph node metastasis status) of breast cancer. In the expression of ER and PR, the Kapp value was substantially higher, whereas the Dapp value was considerably lower, in the positive group than in the negative groups. This finding aligned with the results reported by Huang et al. [27]. We observed that the expression of APT SI value in the HER2-positive group was substantially lower than that in the HER2-negative group. In contrast, the other quantitative parameters showed no considerable variation with differing HER2 expression levels. These findings suggested that the APT SI value exhibited greater sensitivity to HER2-overexpressing breast cancers compared with luminal and triple-negative breast cancers. The correlation between APT SI values and HER2 expression could

enhance non-invasive prediction of HER-2 status in breast cancer, aiding treatment planning. Future research may focus on using APT imaging as a diagnostic tool for personalized treatment strategies and monitoring treatment responses in HER-2 positive cases. Our study also demonstrated that the ADC value was considerably lower in the ER- and PR-positive groups than in the ER- and PR-negative groups, which was not reported in previous studies [27, 28]. This result suggested that ADC values exhibited higher sensitivity in detecting luminal breast cancer. This was because luminal breast cancer was more likely to exhibit the presence of ER, PR, or both on the cell surface, whereas HER-2-positive and triple-negative breast cancer cells lacked the expression of ER and PR. Regarding the expression of Ki-67, we observed no substantial differences in several quantitative parameters between the negative and positive groups. This could be

Table 6 ROC analysis of the diagnostic efficacy of the parameters for the prognostic factors of breast cancer

Factors	Multi parameters	AUC (95%)	P value	Youden index	Sensitivity (%)	Specificity(%)
ER	Kapp	0.695 (0.597–0.794)	0.001	0.361	51.3	84.8
	Dapp	0.690 (0.582–0.797)	0.002	0.367	70.0	66.7
	MTRasym	0.541 (0.426–0.656)	0.495	0.18	51.3	66.7
	ADC	0.677 (0.568–0.785)	0.003	0.26	77.5	48.5
PR	Kapp	0.651 (0.548–0.755)	0.009	0.262	77.6	48.6
	Dapp	0.638 (0.529–0.747)	0.018	0.279	68.4	59.5
	MTRasym	0.524 (0.412–0.636)	0.057	0.142	25.0	89.2
	ADC	0.665 (0.561–0.768)	0.005	0.287	39.5	89.2
HER-2	Kapp	0.650 (0.541–0.759)	0.027	0.369	91.3	45.6
	Dapp	0.650 (0.533–0.767)	0.027	0.263	69.6	56.7
	MTRasym	0.645 (0.526–0.764)	0.033	0.269	91.3	35.6
	ADC	0.699 (0.574–0.823)	0.003	0.352	65.2	70.0
Lymph node status	Kapp	0.596 (0.481–0.712)	0.099	0.271	73.0	54.1
	Dapp	0.546 (0.432–0.661)	0.427	0.163	54.1	62.2
	MTRasym	0.508 (0.394–0.622)	0.895	0.108	21.6	89.2
	ADC	0.629 (0.518–0.741)	0.027	0.23	50.0	73.0

Note Lymph node metastasis status was categorized as positive when lymph node metastases were present and negative when lymph node metastases were absent. No considerable difference in AUCs of other parameters and methods was noted

ADC, apparent diffusion coefficient; APT, amide proton transfer; AUC, area under the curve; ER, estrogen receptor; Dapp, apparent diffusivity; DKI, diffusion kurtosis imaging; HER-2, human epidermal growth factor receptor-2; Kapp, apparent kurtosis coefficient; MTRasym (3.5 ppm), asymmetric magnetization transfer ratio at 3.5 ppm

because our study included more patients with positive Ki-67 expression (92 patients) than those with negative Ki-67 expression (21 patients). This difference might have skewed the results and led to inaccuracies.

In conclusion, our study expanded the application of APTWI and DKI imaging to a novel area, highlighting their respective capabilities and advantages. From a practical standpoint, APTWI and DKI imaging have the following advantages: They can be used in patients who are allergic to MRI contrast agents. Furthermore, the use of these novel scanning sequences minimizes the risk of allergic reactions or adverse effects from contrast agents and lowers the risk of renal damage in patients with renal impairment.

Our study had certain limitations. First, the number of participants was small, and it was a single-center study. Second, the area of interest was delineated only at the level of the largest lesion and sections above and below that level (not the entire lesion), which might have introduced bias. Third, the imaging time of APTWI and DKI was longer than that of the traditional scan sequences, which might have caused discomfort to the participants and affected the quality of the images.

Conclusions

In evaluating breast disease with MRI, APTWI helped distinguish benign from malignant diseases and provided additional information to improve the outcome of diffusion-weighted MRI. However, APTWI failed to demonstrate improved diagnostic efficacy compared to DKI and DWI in differentiating the molecular subtypes of breast

cancer. Future prospective studies should include larger sample sizes from multiple centers to verify the stability and reproducibility of these results.

Abbreviations

ADC	Apparent Diffusion Coefficient
APT SI	Amide Proton Transfer Signal Intensity
APTWI	Amide Proton Transfer-weighted Imaging
MD	Mean Diffusivity
MK	Mean Kurtosis
DKI	Diffusion Kurtosis Imaging
DWI	Diffusion-Weighted Imaging
ER	Estrogen Receptor
PR	Progesterone Receptor
HER-2	Human Epidermal Growth Factor Receptor-2
MTRasym (3.5 ppm)	Asymmetric Magnetization Transfer Ratio at 3.5 ppm

Author contributions

Shan HY and Bao SS contributed to writing the original draft; Ke TF and Liu YF contributed to the scanning magnetic resonance imaging data; Xie Y, Zheng GR and Li GC analyzed the data; Liao CD and Yang J contributed to conceptualization and checking the data; Tan N and Zhou XY contributed to image post-processing. All authors contributed to the article and approved the submitted version. The authors wish to thank Xu YZ, an employee of Philips Healthcare, for her kind help in the statistical analysis.

Funding

This study was supported by the National Natural Science Foundation of China (grant no. 82060313, 82160340), the joint project of basic research of Kunming Medical University and Department of Science and Technology of Yunnan Province (202301AY070001-243, 202201AY070001-148), Yunnan Talents Support Program (grant number XDYC-MY-2022-0064), the Scientific Research Fund Project of Education Department of Yunnan Province (2023Y0818), the Outstanding Youth Science Foundation of Yunnan Basic Research Project (202201AW070002), First-Class Discipline Team of Kunming Medical University (2024XKTDTS03).

Data availability

No datasets were generated or analysed during the current study.

Declarations

Ethical approval

This study was performed in accordance with the ethical standards laid down in the 1964 Declaration of Helsinki (Revised in 2013). It was approved by the ethics committee of the Yunnan Cancer Hospital (KYLX2023-110). All methods were carried out according to relevant guidelines and regulations.

Consent for participation

Several study participants or cohorts have been previously reported in Radiology.

Informed consent

All patients provided written informed consent prior to undergoing the MRI scan.

Guarantor

The scientific guarantor of this publication is Jun Yang.

Statistics and Biometry

Yongzhou Xu kindly provided statistical advice for this manuscript. No complex statistical methods were necessary for this study.

Methodology

Retrospective; Case-control study; Performed at one institution.

Competing interests

The authors declare no competing interests.

Received: 25 August 2024 / Accepted: 26 November 2024

Published online: 18 December 2024

References

- Britt KL, Cuzick J, Phillips KA. Key steps for effective breast Cancer Prevention. *Nat Rev Cancer*. 2020;20(8):417–36. <https://doi.org/10.1038/s41568-020-0266-x>. Epub 2020/06/13.
- Sung H, Ferlay J, Siegel RL, Laversanne M, Soerjomataram I, Jemal A et al. Global Cancer Statistics. 2020: Globocan Estimates of Incidence and Mortality Worldwide for 36 Cancers in 185 Countries. *CA: a cancer journal for clinicians* (2021) 71(3):209–49. Epub 2021/02/05. <https://doi.org/10.3322/caac.21660>
- López-Ruiz JA, Mieza JA, Zabalza I, Vivanco MDM. Comparison of Genomic Profiling Data with Clinical Parameters: Implications for Breast Cancer Prognosis. *Cancers* (2022) 14(17). Epub 2022/09/10. <https://doi.org/10.3390/cancers14174197>
- Goldhirsch A, Wood WC, Coates AS, Gelber RD, Thürlimann B, Senn HJ, on the Primary Therapy of Early Breast Cancer. Strategies for Subtypes—Dealing with the Diversity of Breast Cancer: Highlights of the St. Gallen International Expert Consensus 2011. *Annals of oncology: official journal of the European Society for Medical Oncology* (2011) 22(8):1736–47. Epub 2011/06/29. <https://doi.org/10.1093/annonc/mdr304>
- Jensen JH, Helpert JA, Ramani A, Lu H, Kaczynski K. Diffusional Kurtosis Imaging: the quantification of Non-gaussian Water Diffusion by means of magnetic resonance imaging. *Magn Reson Med*. 2005;53(6):1432–40. <https://doi.org/10.1002/mrm.20508>. Epub 2005/05/21.
- Yuan C, Jin F, Guo X, Zhao S, Li W, Guo H. Correlation analysis of breast Cancer dwi combined with Dce-Mri Imaging Features with molecular subtypes and prognostic factors. *J Med Syst*. 2019;43(4):83. <https://doi.org/10.1007/s10916-019-1197-5>. Epub 2019/02/28.
- Li Q, Cao B, Tan Q, Liu K, Jiang S, Zhou J. Prediction of muscle Invasion of bladder Cancer: a comparison between Dki and Conventional Dwi. *Eur J Radiol*. 2021;136:109522. <https://doi.org/10.1016/j.ejrad.2021.109522>. Epub 2021/01/13.
- Yuan L, Lin X, Zhao P, Ma H, Duan S, Sun S. Correlations between Dki and Dwi with Ki-67 in Gastric Adenocarcinoma. *Acta radiologica (Stockholm, Sweden: 1987)* (2023) 64(5):1792–8. Epub 2023/02/07. <https://doi.org/10.1177/02841851231153035>
- Rosenkrantz AB, Padhani AR, Chenevert TL, Koh DM, De Keyzer F, Taouli B, et al. Body diffusion kurtosis imaging: basic principles, applications, and considerations for clinical practice. *J Magn Reson Imaging*. 2015;42(5):1190–202. <https://doi.org/10.1002/jmri.24985>. Epub 2015/06/30.
- Xue Y, Zhang Z, Wen C, Liu H, Wang S, Li J, et al. Characterization of Alzheimer's Disease using Ultra-high B-Values apparent diffusion coefficient and diffusion kurtosis imaging. *Aging Disease*. 2019;10(5):1026–36. <https://doi.org/10.14336/ad.2018.1129>. Epub 2019/10/09.
- Wu B, Jia F, Li X, Zhang M, Han D, Jia Z. Amide Proton transfer imaging vs Diffusion Kurtosis Imaging for Predicting histological Grade of Hepatocellular Carcinoma. *J Hepatocellular Carcinoma*. 2020;7(159–68). <https://doi.org/10.2147/jhc.S272535>. Epub 2020/10/30.
- Yin H, Wang D, Yan R, Jin X, Hu Y, Zhai Z, et al. Comparison of Diffusion Kurtosis Imaging and Amide Proton Transfer Imaging in the diagnosis and Risk Assessment of prostate Cancer. *Front Oncol*. 2021;11:640906. <https://doi.org/10.3389/fonc.2021.640906>. Epub 2021/05/04.
- Chen T, Li Y, Lu SS, Zhang YD, Wang XN, Luo CY et al. Quantitative evaluation of diffusion-kurtosis imaging for grading endometrial carcinoma: a comparative study with diffusion-weighted imaging. *Clinical radiology* (2017) 72(11):995.e111–e20. Epub 2017/08/05. <https://doi.org/10.1016/j.crad.2017.07.004>
- Zhou J, Payen JF, Wilson DA, Traystman RJ, van Zijl PC. Using the Amide Proton Signals of Intracellular Proteins and peptides to detect Ph effects in Mri. *Nat Med*. 2003;9(8):1085–90. <https://doi.org/10.1038/nm907>. Epub 2003/07/23.
- Zhou J, Blakeley JO, Hua J, Kim M, Laterra J, Pomper MG, et al. Practical Data Acquisition Method for Human Brain Tumor Amide Proton Transfer (apt) imaging. *Magn Reson Med*. 2008;60(4):842–9. <https://doi.org/10.1002/mrm.21712>. Epub 2008/09/26.
- Sun PZ, Zhou J, Sun W, Huang J, van Zijl PC. Detection of the ischemic Penumbra using Ph-Weighted mri. *J Cereb Blood flow Metabolism: Official J Int Soc Cereb Blood Flow Metabolism*. 2007;27(6):1129–36. <https://doi.org/10.1016/j.jcbfm.2007.06.004>. Epub 2006/11/30.
- McVicar N, Li AX, Gonçalves DF, Bellyou M, Meakin SO, Prado MA, et al. Quantitative tissue Ph measurement during cerebral ischemia using Amine and Amide Concentration-Independent detection (acid) with mri. *J Cereb Blood flow Metabolism: Official J Int Soc Cereb Blood Flow Metabolism*. 2014;34(4):690–8. <https://doi.org/10.1038/jcbfm.2014.12>. Epub 2014/02/06.
- Park YH, Senkus-Konefka E, Im SA, Pentheroudakis G, Saji S, Gupta S, et al. Pan-asian adapted esmo clinical practice guidelines for the management of patients with early breast Cancer: a ksmo-esmo Initiative endorsed by CSCO, ISMPO, JSMO, MOS, SSO and TOS. *Annals Oncology: Official J Eur Soc Med Oncol*. 2020;31(4):451–69. <https://doi.org/10.1016/j.annonc.2020.01.008>. Epub 2020/02/23.
- Balthazar P, Tajmir SH, Ortiz DA, Herse CC, Shea LAG, Seals KF et al. The Artificial Intelligence Journal Club (#Radaij): A Multi-Institutional Resident-Driven Web-Based Educational Initiative. *Academic radiology* (2020) 27(1):136–9. Epub 2019/11/07. <https://doi.org/10.1016/j.acra.2019.10.005>
- Hammond ME, Hayes DF, Wolff AC, Mangu PB, Temin S. American Society of Clinical Oncology/College of American Pathologists Guideline Recommendations for Immunohistochemical Testing of Estrogen and progesterone receptors in breast Cancer. *J Oncol Pract*. 2010;6(4):195–7. <https://doi.org/10.1200/jop.777003>. Epub 2010/11/03.
- Wolff AC, Hammond ME, Hicks DG, Dowsett M, McShane LM, Allison KH, et al. Recommendations for Human Epidermal Growth Factor Receptor 2 testing in breast Cancer: American Society of Clinical Oncology/College of American Pathologists Clinical Practice Guideline Update. *J Clin Oncology: Official J Am Soc Clin Oncol*. 2013;31(31):3997–4013. <https://doi.org/10.1200/jco.2013.50.984>. Epub 2013/10/09.
- Goldhirsch A, Winer EP, Coates AS, Gelber RD, Piccart-Gebhart M, Thürlimann B, et al. Personalizing the treatment of women with early breast Cancer: highlights of the St Gallen International Expert Consensus on the primary therapy of early breast Cancer 2013. *Annals Oncology: Official J Eur Soc Med Oncol*. 2013;24(9):2206–23. <https://doi.org/10.1093/annonc/mdt303>. Epub 2013/08/07.
- Chen W, Li L, Yan Z, Hu S, Feng J, Liu G, et al. Three-dimension Amide Proton transfer mri of rectal adenocarcinoma: correlation with pathologic prognostic factors and comparison with Diffusion Kurtosis Imaging. *Eur Radiol*. 2021;31(5):3286–96. <https://doi.org/10.1007/s00330-020-07397-1>. Epub 2020/10/31.
- Meng N, Wang X, Sun J, Han D, Bai Y, Wei W, et al. A comparative study of the Value of Amide Proton Transfer-Weighted Imaging and Diffusion Kurtosis Imaging in the diagnosis and evaluation of breast Cancer. *Eur Radiol*. 2021;31(3):1707–17. <https://doi.org/10.1007/s00330-020-07169-x>. Epub 2020/09/06.

25. Li T, Hong Y, Kong D, Li K. Histogram Analysis of Diffusion Kurtosis Imaging based on whole-volume images of breast lesions. *J Magn Reson Imaging*. 2020;51(2):627–34. <https://doi.org/10.1002/jmri.26884>. Epub 2019/08/07.
26. Gao W, Zhang S, Guo J, Wei X, Li X, Diao Y, et al. Investigation of Synthetic Relaxometry and Diffusion measures in the differentiation of Benign and malignant breast lesions as compared to bi-rads. *J Magn Reson Imaging*. 2021;53(4):1118–27. <https://doi.org/10.1002/jmri.27435>. Epub 2020/11/13.
27. Huang Y, Lin Y, Hu W, Ma C, Lin W, Wang Z, et al. Diffusion kurtosis at 3.0t as an in vivo imaging marker for breast Cancer characterization: correlation with prognostic factors. *J Magn Reson Imaging*. 2019;49(3):845–56. <https://doi.org/10.1002/jmri.26249>. Epub 2018/09/28.
28. Kang HS, Kim JY, Kim JJ, Kim S, Lee NK, Lee JW, et al. Diffusion kurtosis Mr Imaging of invasive breast Cancer: correlations with prognostic factors and molecular subtypes. *J Magn Reson Imaging*. 2022;56(1):110–20. <https://doi.org/10.1002/jmri.27999>. Epub 2021/11/19.

Publisher's note

Springer Nature remains neutral with regard to jurisdictional claims in published maps and institutional affiliations.